processes

MDPI

*Technical Note*

# Research on $CO_2$ Quasi-Dry Fracturing Technology and Reservoir $CO_2$ Distribution Pattern

**Wei Yang, Meilong Fu *, Yanping Wang, Jianqiang Lu and Guojun Li**

Hubei Key Laboratory of Oil and Gas Drilling and Production Engineering, College of Petroleum Engineering, Yangtze University, Wuhan 430100, China; 15527310185@163.com (W.Y.)
* Correspondence: fmlytze@163.com

**Abstract:** $CO_2$ fracturing technology has been widely used to develop unconventional oil and gas reservoirs such as shale oil and gas and tight sandstone reservoirs. To mitigate the issues of low viscosity and high friction associated with traditional $CO_2$ fracturing technology, this paper proposes $CO_2$ quasi-dry fracturing technology. Taking the low permeability tight sandstone reservoir in Block X of T oilfield as the research object, indoor experiments were conducted to optimize the ratio of $CO_2$ quasi-dry fracturing fluid. Numerical simulation was used to select the optimal construction displacement using FracproPT, and the temperature and pressure changes in the reservoir and the grid after $CO_2$ injection were analyzed using CMG to lay a foundation for the production practice. The results show that the fracturing fluid formulation system is 70% liquid $CO_2$ + 30% water with 1.2% water-based thickener APQD-6 and 1.2% $CO_2$ thickener APFR-2; the optimal construction displacement is 3 $m^3$/min, and the fracture half-length is 206.2 m; the reservoir temperature responds to the $CO_2$ injection volume more rapidly than the pressure, which indicates that $CO_2$ has a more significant effect on the temperature. The field application results show that the reservoir temperature responds more rapidly to the $CO_2$ injection volume than the pressure, indicating that $CO_2$ has a more significant effect on temperature. The field application results are remarkable. This operation successfully achieved the key parameter indicators of the highest sand ratio of 10% and the average sand ratio of 6%. The daily liquid production of the well was stable at 1.6 t, the daily gas production jumped by 820 $m^3$, and the daily oil production also increased by 0.7 t. The effect of single-well stimulation is very prominent, which strongly verifies the feasibility and effectiveness of $CO_2$ quasi-dry fracturing technology exploiting low-porosity and low-permeability reservoirs. This practical result provides valuable practical guidance for developing similar reservoirs. It is expected to promote the further development and application of low porosity and low permeability reservoir development technology.

**Keywords:** low permeability tight sandstone reservoir; carbon dioxide quasi-dry fracturing; fracturing fluid formulation system; fracturing parameter optimization; reservoir $CO_2$ study; CCS TE348; literature symbol code

check for updates

Academic Editor: Qingbang Meng

Received: 2 January 2025
Revised: 27 January 2025
Accepted: 2 February 2025
Published: 8 February 2025

**Citation:** Yang, W.; Fu, M.; Wang, Y.; Lu, J.; Li, G. Research on $CO_2$ Quasi-Dry Fracturing Technology and Reservoir $CO_2$ Distribution Pattern. *Processes* **2025**, *13*, 472. https://doi.org/10.3390/pr13020472

**Copyright:** © 2025 by the authors. Licensee MDPI, Basel, Switzerland. This article is an open access article distributed under the terms and conditions of the Creative Commons Attribution (CC BY) license (https://creativecommons.org/licenses/by/4.0/).

## 1. Introduction

Tight sandstone reservoirs have poor physical properties and high clay mineral content, and conventional hydraulic fracturing is prone to cause water sensitivity and hydro-locking, affecting production enhancement [1]. Liquid $CO_2$ has technical advantages over hydraulic fracturing, such as low injury, cleanliness, and environmental protection [2,3]. Its most significant advantage lies in the fact that liquid $CO_2$ fracturing can reduce the damage to

formation conductivity caused by the residual fluid and filter cake of fracturing fluid. Pure liquid $CO_2$ fracturing was first proposed in Canada, and $CO_2$ fracturing was first used in North America for unconventional oil and gas reservoirs in the late 1980s, during which more than 1000 wells were implemented with liquid $CO_2$ fracturing [4]. In the following years, $CO_2$ fracturing was applied to more than 30 oil and gas reservoirs, of which 95% were gas wells and 5% were oil wells. Domestic liquid $CO_2$ fracturing research began in the 21st century, and in recent years, fewer field applications have been made, and it is still in the experimental stage [5–8]. In 2013, the first domestic $CO_2$ dry sand-added fracturing test was carried out in the Sudong 44–22 well in Changqing gas field with a volume of 2.8 $m^3$ of sand added, an average sand ratio of 3.48%, and a maximum transient sand ratio of 9%, which achieved good results. The technology has been applied in 15 wells in the Sulige gas field, which can meet conventional vertical wells/directional wells' engineering operation needs and achieve the maximum single sand volume of 30 $m^3$ and the maximum sand ratio of 22% [9]. The pilot experiment of $CO_2$ quasi-dry method technology was carried out in Daqing Oilfield. After fracturing, the oil production of a single well was 6.8 t, and the effect of increasing oil production was noticeable [10].

Although scholars have made some progress in the research of $CO_2$ dry fracturing, there are still some deficiencies in liquid $CO_2$ fracturing: low viscosity, poor sand-carrying, and loss-reducing ability; high friction resistance, great difficulty in effective fracture creation; and limited scale of sand addition by special closed sand adding equipment. The above shortcomings lead to ① the poor performance of liquid $CO_2$ in terms of thickening, drag reduction, and sand carrying, which makes it challenging to achieve the ideal effect of production increase; ② the high cost of fracturing equipment, which makes it challenging to promote. To solve the above problems, Beijing Aipu Polymerisation Technology Co., Ltd., Beijing, China proposed $CO_2$ quasi-dry fracturing technology [11]. This technology adopts the combination of conventional water-based fracturing and $CO_2$ fracturing. Compared with $CO_2$ pure dry fracturing, $CO_2$ quasi-dry fracturing has the following advantages: (1) no need to use special closed sand mixing equipment, simple operation and control, and can meet large-scale sand fracturing; (2) the use of a small amount of water phase configuration into water-based sand-carrying fluid, the reservoir damage is very low, the effect of increasing production is excellent, and the cost performance is high. (3) $CO_2$ quasi-dry fracturing fluid is a structural fluid with good viscoelasticity, excellent temperature, and shear resistance. (4) The drag reduction and sand-carrying integration can be realized, and the drag-reduction fluid and sand-carrying fluid can be prepared at the same time. However, there are also disadvantages, such as difficult phase control, high construction parameter requirements, and limited scope of application. The process is based on $CO_2$ and water (the ratio of water/carbon is generally not more than 40:60), adding water-based thickener APQD-6 and $CO_2$ thickener APFR-2 to form a mixture with a specific viscosity, injecting it with a large displacement using a high-pressure pump on the ground, creating a dynamic fracture in the formation, and then filling the proppant into the fracture, which can provide a seepage channel with high permeability for oil and gas transport and realize production enhancement and transformation. In recent years, important technical breakthroughs have been made in the oilfield production site, and the experimental work of supercritical $CO_2$ quasi-dry fracturing technology for sandstone reservoirs has been successfully carried out [12–14].

Therefore, this paper takes $CO_2$ quasi-dry fracturing as the research direction, combines physical simulation and numerical simulation as the innovation point, takes Block X of T oilfield as an example, and selects the fracturing fluid formulation system preferably through physical simulation experiments. It uses FracproPT 2011 software to optimize the construction displacement and CMG 2021 software to study the effect on reservoir

temperature and pressure after injecting $CO_2$, comparing the effect analysis before and after fracturing to achieve the production increase target and lay the theoretical foundation for production practice.

## 2. Oilfield Overview

The T oil field is located north of the central uplift zone of the Dongpu depression, and the whole field is a succession of middle depression and uplift tectonics. The depth of the oil reservoir is 2900~3600 m. The primary lithology is light gray quartz siltstone with a small amount of fine siltstone. The rock cement content is high, including gray, mud, and dolomite. In terms of cementation type, it is mainly of pore type, which is followed by contact-pore type. The physical properties of the crude oil are good, with low density, viscosity, and sulfur content. The compression coefficient of crude oil is $13.0 \times 10^{-4}$ $MPa^{-1}$, and the original gas–oil ratio is 184 $m^3/t$. In addition, the mineralization of formation water is high at 25~33 $\times$ $10^4$ mg/L, and the water type is dominated by $CaCl_2$ type.

Block X is an important oil-bearing fault block in the T oilfield, and its oil geological reserve is as high as 161.36 $\times$ $10^4$ t. Regarding geographical distribution, it is mainly concentrated in the high-value area of tectonics, and it is subject to multiple factors such as tectonics and lithology. The porosity of the reservoir is in the range of 7.8% to 16.8%. At the same time, the permeability is about 0.1 to 10.3 $\times$ $10^{-3}$ $\mu m^2$, so it is a tectonic-rocky reservoir with low porosity, low permeability, and low viscosity complicated by faults.

## 3. Optimization of $CO_2$ Quasi-Dry Fracturing Fluid Ratio

In the $CO_2$ quasi-dry fracturing process, the performance of the fracturing fluid directly determines the success or failure of the process. This process requires that liquid $CO_2$ mixed with water can form a homogeneous and stable mixed phase; simultaneously, the fracturing fluid system must have a specific viscosity to meet the needs of seam formation and sand transport. For this reason, it is vital to optimize the solvent dosage ratio of the fracturing fluid [15].

### *3.1. Optimization of APFR-2+APQD-6 Dosage Ratio*

Under the temperature and pressure conditions of the actual construction process, the low viscosity of carbon dioxide will lead to a severe lack of sand-carrying performance, so it is necessary to add a thickener to improve the viscosity of the fracturing fluid to improve the sand-carrying capacity. APQD-6 and APFR-2 are integrated self-crosslinking emulsion fracturing fluid thickeners and dry fracturing fluid drag-reducing thickeners, respectively. APQD-6 has strong viscoelasticity and excellent sand-suspension performance, which meets the requirements of water-based sand-carrying and water-based sand-carrying requirements. APFR-2 is made from monomers such as ethyl propylene ether, methyl methacrylate, octadecyl methacrylate, and allyl methyl carbonate, which are copolymerized in a pro-carbon dioxide solvent [16]. It possesses excellent temperature shear resistance and drag reduction effect, so APFR-2+APQD-6 was used as the solvent for $CO_2$ quasi-dry fracturing fluid.

The APFR-2+APQD-6 dosage ratio was optimized to further improve the fracturing fluid's sand-carrying and drag-reducing integrated construction ability. In the experiment, a certain amount of water and $CO_2$ and different concentration ratios of APFR-2+APQD-6 were added to the system. Then, a ZNN-D6S digital six-speed rotational viscometer was used to test the viscosity data at a 170 $s^{-1}$ shear rate and different temperatures, as shown in Table 1.

**Table 1.** Viscosity data at different concentration ratios at different temperatures (mPa·s).

| Different Concentration Ratio | 28 °C | 45 °C | 60 °C | 80 °C |
|---|---|---|---|---|
| 1.0% + 1.0% | 43.25 | 32.16 | 26.39 | 19.31 |
| 1.2% + 1.2% | 63.7 | 58.25 | 44.22 | 35.13 |
| 1.5% + 1.5% | 153.25 | 132.64 | 109.35 | 95.28 |

Requirements of fracturing fluid formulation and system viscosity ≥ 20 mPa-s. Table 1 shows that the system viscosity values of 1.2%APFR-2+1.2%APQD-6 and 1.5%APFR-2+1.5%APQD-6 satisfy the requirements of fracturing fluids. Still, the latter has a higher concentration. Given the consideration of the construction cost, 1.2%APFR-2+1.2%APQD-6 was selected as the dosage ratio.

### *3.2. Optimization of Liquid $CO_2$ + Water Dosage Ratio*

Liquid $CO_2$ is a weak solvent that is not soluble in water, so it is necessary to mix a small amount of water-based fracturing fluid with liquid $CO_2$ to carry sand. Therefore, it is very imperative to optimize the ratio of water to carbon in the fracturing fluid. By optimizing the ratio of liquid $CO_2$ to water base, the performance of fracturing fluid can be stabilized. In the laboratory simulation experiment, the shear rate was set at 170 $s^{-1}$. The viscosity at 170 $s^{-1}$ shear rate was tested using a ZNN-D6S digital six-speed rotational viscometer at different water–carbon ratios and temperatures, and the results are shown in Table 2.

**Table 2.** Viscosity data at different temperatures with different water-carbon ratios (1.2% APFR-2 + 1.2% APQD-6) (mPa·s).

| The Ratio of Water to Carbon | 28 °C | 45 °C | 60 °C | 80 °C |
|---|---|---|---|---|
| 20:80 | 63.82 | 58.58 | 44.53 | 35.67 |
| 30:70 | 52.6 | 43.43 | 32.26 | 25.39 |
| 40:60 | 50.82 | 39.56 | 26.53 | 17.53 |

From the experimental results in Table 2, it can be seen that the viscosity of the 1.2%APFR-2+1.2%APQD-6 formulation system is 25.39 mPa·s when the temperature is 80 °C, and the water–carbon ratio is 30:70, which can meet the sand-carrying requirement. The bonded water can be formed under this condition to maintain the characteristics of $CO_2$ dry fracturing fluids, and the viscosity of the system is too high when the water–carbon ratio is 20:80, which will lead to a cost increase. Therefore, the optimal water–carbon ratio is 30:70. In summary, the fracturing fluid formulation system is 70% liquid $CO_2$ + 30% water, with 1.2% APQD-6 and 1.2% APFR-2, which can meet the fracturing performance requirements.

## 4. Optimization of Fracturing Parameters

Block X of the T oilfield comprises non-acid-sensitive, low-porosity, and low-permeability reservoirs with 73% oil saturation. The reservoir has 73.1% oil saturation and good oil and gas content, which makes it suitable for $CO_2$ quasi-dry fracturing. The P1 well is a production well located in Block X, which is exploited by straight well fracturing. The optimization method of $CO_2$ quasi-dry fracturing construction parameters is studied from the perspective of construction displacement, aiming to ensure the smooth implementation of fracturing construction.

*Optimization of Construction Volume*

Fracturing construction displacement is a key factor affecting fracture height and construction safety. If the construction displacement is too large, it easily leads to compartment

cracking and a fracture height that is too high. When the displacement is too small, the operation cycle will be longer, the transport efficiency of sand-carrying fluids will be reduced, and it is easy for sand blockage and other safety hazards to appear during the injection process [17]. In this paper, the scale of liquid $CO_2$ is formulated as 600 $m^3$. FracproPT software is used to study the fracture parameters under different construction displacements. The relationship between construction displacements and fracture half-length, as well as the causeless inflow capacity, is shown in Figure 1.

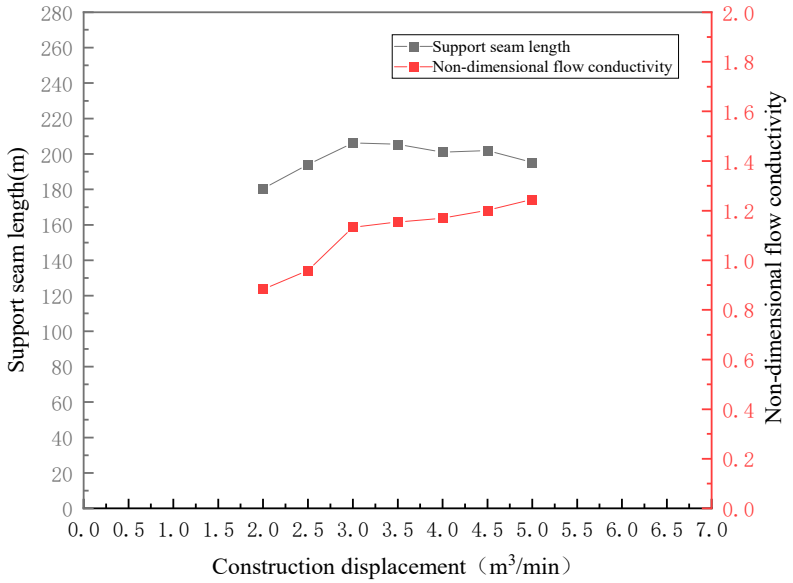



**Figure 1.** Relationship between construction displacement and support joint length and dimensionless conductivity.

It can be seen from Figure 1 that the half-length of the crack shows a tendency to increase and then decrease with the increase in construction displacement. When the construction displacement is 3 $m^3$/min, the crack half-length reaches a peak of 206.2 m. At the same time, as the crack width increases, the uncaused hydraulic capacity also rises, reaching 1.133. At this time, the crack half-length and the uncaused hydraulic capacity have reached a more desirable state. When the construction displacement is greater than 3 $m^3$/min, the trend of increasing the uncaused flow capacity begins to slow down. Using a small displacement for construction may limit crack expansion due to insufficient seam formation; increasing the construction displacement can effectively reduce the crack initiation time, but the requirement for equipment is higher. Therefore, the preferred construction displacement is 3 $m^3$/min, taking into account the growth of the causeless inflow capacity and fracture half-length as well as the filtration loss of fracturing fluid.

When the construction displacement of 3 $m^3$/min is selected, the sand spreading concentration inside the fracture is simulated using FracproPT software, as shown in the two-dimensional plane in Figure 2; for the upper coordinate is crack length, the unit is m, the lower coordinate is proppant concentration, and the unit is kg/$m^2$. The specific data are shown in Table 3, and the different colors represent the changes in the proppant spreading concentration. The fracture morphology with a more significant concentration of proppant can form an effective and high conductivity, thus realizing the reservoir modification [18].

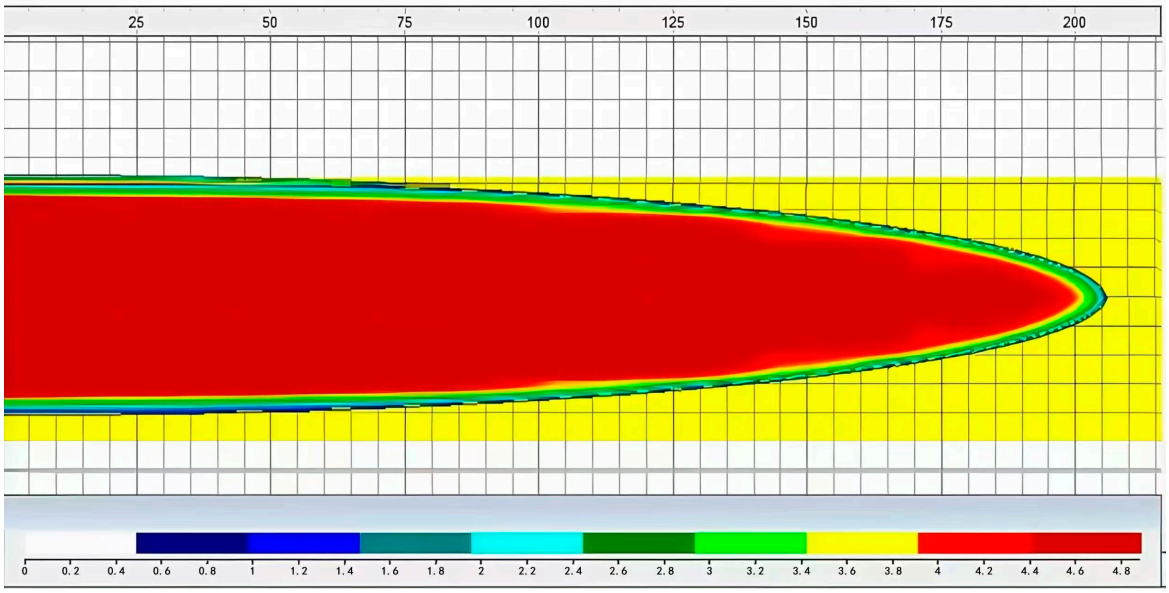



**Figure 2.** When the construction displacement is 3 $m^3$/min, the sand concentration inside the crack is laid.

**Table 3.** Proppant concentration in fracture.

| Data Name | Numerical Value |
|---|---|
| Crack length (m) | 206.2 |
| Support seam length (m) | 206.2 |
| Total crack height (m) | 42.5 |
| Total height of supporting crack (m) | 42.5 |
| The depth of the top of the crack (m) | 3473.3 |
| Depth at the bottom of the crack (m) | 3515.8 |
| Mean crack width (cm) | 0.885 |
| Average proppant concentration (kg/$m^2$) | 6.70 |
| Equivalent number of multiple fractures | 1.0 |
| Non-dimensional flow conductivity | 1.333 |

From Figure 2, we can see the change in the position inside the fracture when the average proppant concentration is 6.7 kg/$m^2$; the fracture half-length, proppant half-length, proppant height, and average fracture width are 206.2 m, 206.2 m, 42.5 m and 0.885 cm, respectively. The higher the proppant concentration in the middle of the fracture, the larger the proppant width is, the lower the energy consumed by the formation fluid when it passes through the fracture, and the higher the hydraulic conductivity, accordingly; on the contrary, when the fracture expands from the near-wellbore zone to the surrounding area, the sand-carrying capacity of the fracturing fluid gradually decreases, and the lower the concentration of the proppant spreading sand in the two ends of the fracture is, the lower the hydraulic conductivity is.

Based on the above simulation results, the half-length of the fracture and the inflow capacity obtained from the simulation were taken as the key measurement factors for the fracturing optimization results. At the construction displacement of 3 $m^3$/min, the fracture inflow capacity profile obtained from the simulation of fracturing construction using FracproPT software is shown in Figure 3; the specific data are shown in Table 4. The coordinate above is fracture length, whose unit is m, and the coordinate below is fracture conductivity, whose unit is mD m.

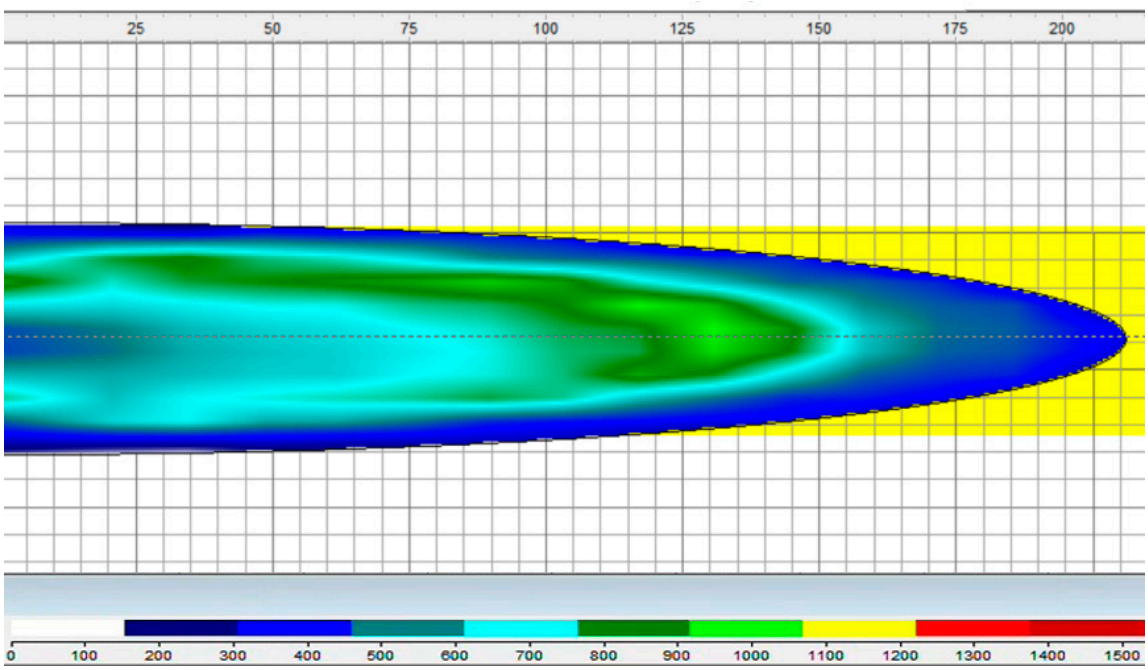



**Figure 3.** Schematic diagram of the well tight sandstone reservoir fracturing fracture conductivity results for P1.

**Table 4.** Fracture flow conductivity.

| Data Name | Numerical Value |
|---|---|
| Crack length (m) | 206.3 |
| Support seam length (m) | 206.3 |
| Total crack height (m) | 42.6 |
| Total height of supporting crack (m) | 42.6 |
| The depth of the top of the crack (m) | 3473.3 |
| Depth at the bottom of the crack(m) | 3515.8 |
| Mean crack width (m) | 0.922 |
| Average proppant concentration (kg/m$^2$) | 7.02 |
| Equivalent number of multiple fractures | 1.0 |
| Non-dimensional flow conductivity | 1.157 |

As shown in Figure 3, the fracture flow conductivity of the optimized fracture is 302.92 mD·m, and the half-length of the fracture is 206 m. The closer the fracture is to the area near the wellbore, the looser the internal structure is, which leads to higher porosity; at the same time, the connectivity between the fracture is better so that the fluid can flow more smoothly. They are subjected to less resistance and therefore have a higher flow conductivity; this indicates that the fracturing simulation is good. The effect is good, which provides a reliable basis for the field construction of $CO_2$ quasi-dry fracturing.

## 5. Reservoir $CO_2$ Distribution and Reach

The porosity of the oil reservoir in Block X of T oilfield is about 7.8%~16.8%, and the permeability is about 0.1~10.3 × $10^{-3}$ μm$^2$. Given this, the method of 'straight well + $CO_2$ quasi-dry fracturing' is adopted for development. CMG's STARS model was used to analyze the change rules of pressure and temperature in the near-well zone of the reservoir after $CO_2$ injection to provide a basis for the subsequent analysis of the reservoir sensitivity parameter model [19,20].

### 5.1. $CO_2$ Distribution in Reservoir

During the underground fracturing operation, the injected $CO_2$ will undergo a phase change from a liquid state to a supercritical state. This phase change leads to a continuous expansion of its volume, which produces a pressurization effect and promotes fracture generation. For this purpose, temperature and pressure variations in the reservoir and grid are analyzed.

The parameters are set as follows: the formation pressure is 48.6 MPa, temperature is 120 °C, wellhead temperature is 121.6 °C, wellhead $CO_2$ injection displacement is 3 $m^3/s$, and gas injection flow rate of the injection well is 340,000 $m^3/d$.

Temperature and Pressure of Reservoir in Near-Well Zone and Far-Well Zone

Due to the throttling effect of $CO_2$ and the heat exchange with the surrounding rock, the temperature of the near-well zone shows a certain degree of decreasing trend at the beginning. As the fracturing progresses, the pressure in the near-well zone gradually stabilizes but remains relatively high. As for the far zone, because it is far away from the wellbore, the effect of $CO_2$ injection is relatively lagging. At the early stage of fracturing, the pressure change in the far-well zone is not apparent, and the temperature change is relatively smooth without the apparent downward trend like that in the near-well zone. The significant difference in reservoir pressure and temperature between the near-well zone and the far-well zone fully shows that $CO_2$ injection significantly affects reservoir temperature and pressure.

$CO_2$ can spread to the whole fracture by its good mobility and diffusivity. Inside the fracture, the presence of $CO_2$ makes the fluid pressure distribution more complicated, and the pressure values at different locations will change continuously with the transport and distribution of $CO_2$. Although $CO_2$ can reach the whole crack, its temperature range is relatively narrow given the heat transfer characteristics of the formation temperature. In the heat transfer process, heat is transferred from the high-temperature formation to the low-temperature $CO_2$ and the surrounding area. However, due to the low thermal conductivity of the formation rock itself, the heat transfer is slow, so the temperature influence is limited to a few meters near the well. Within this range, temperature changes are more pronounced, while beyond this range, temperature changes are minimal.

As can be seen in Figure 4, at the initial stage of $CO_2$ injection accumulation (about 30 days), $CO_2$ is usually injected into the reservoir at high pressure and low temperature, resulting in a rapid decrease in temperature in the near-well zone with a nearly straight-line downward trend and a significant difference from the original temperature of the reservoir. During the injection process, there is a drastic heat exchange between $CO_2$ and the reservoir. Then, the temperature of the reservoir in the near-well zone is basically kept unchanged, presenting a stable straight line, which suggests that there may be an injection accumulation period in a short period, during which the continuous injection of $CO_2$ decreases the temperature of the near-well reservoir until it reaches a relatively stable state. At the initial stage of $CO_2$ injection, the reservoir temperature in the far-well zone remains in the original state because $CO_2$ has not yet diffused to the far-well zone due to the long distance from the injection point. The heat exchange between $CO_2$ and the reservoir in the far-well zone gradually unfolds. The temperature in the far-well zone decreases as the injection volume continues to increase and the time accumulates. At a later stage (around 270 days), the reservoir temperature in the far-well zone gradually decreases, indicating that the injection of $CO_2$ has spread to the far-well zone. At the later stage (until the gas injection is completed), the reservoir temperature in the far well is unchanged, which indicates that the temperature of the reservoir in the far thriving zone reaches a new equilibrium state after the $CO_2$ has sufficiently diffused into the far well zone and has

completed a certain degree of heat exchange with the reservoir. The reservoir pressures of both the near well and the far well decrease gradually with the increase in gas injection, and the pressure change curves of the two wells are basically parallel, which indicates that the decreasing trend is the same. Although there are differences in the spatial locations of the near-well zone and the far-well zone, from an overall point of view, their pressure change trends are affected by the key factor of gas injection volume, and the pressure inside the reservoir shows a gradual decrease with the increasing of gas injection volume.

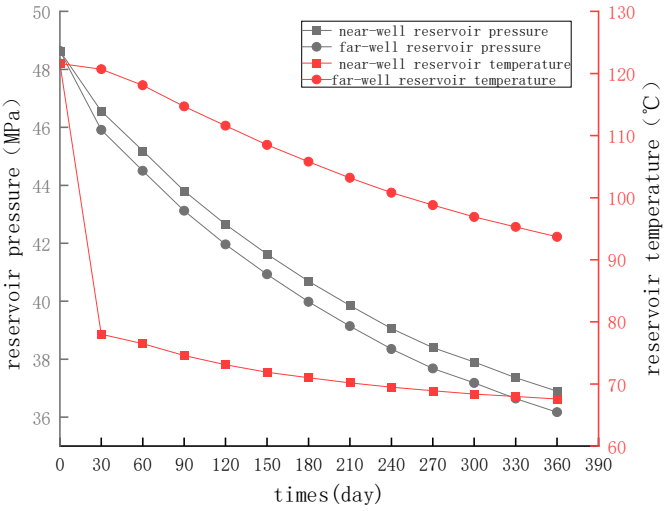
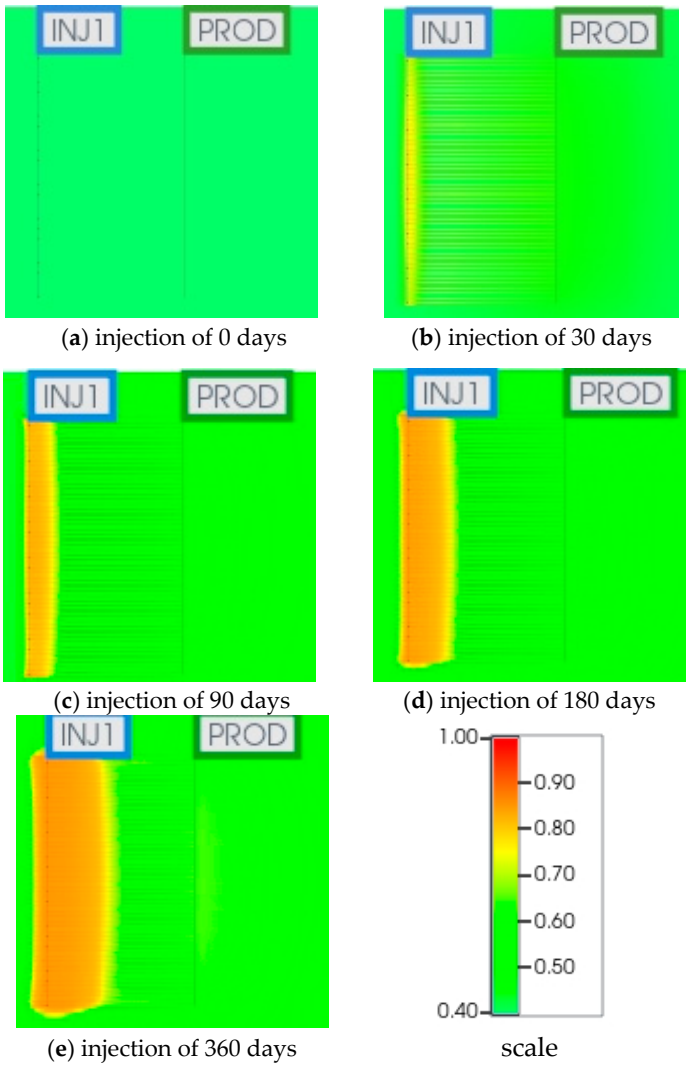



**Figure 4.** Temperature and pressure variation curve of the reservoir in the near-well zone and far-well zone.

In summary, compared with the pressure, the temperature has an enormous influence on the reservoir, and the temperature responds more rapidly to the injection volume; in the early stage of accumulation, the temperature and pressure of the near-well reservoir are susceptible to $CO_2$ injection.

### *5.2. Range of $CO_2$ Diffusion in the Reservoir*

Figure 5 shows the plan view of the $CO_2$ ripple range of the reservoir during fracturing, which increases with the gradual increase in the gas injection volume, which becomes a key factor affecting the degree of $CO_2$ diffusion. When the gas injection volume is small, the $CO_2$ does not completely penetrate the fracture, indicating that sufficient injection volume is needed to create a long seam. Further analysis reveals that the $CO_2$ content of the reservoir is more prominent in the 17.5 m near the well, so when fracturing and reforming in the near-well area, the rock is more straightforward to produce cracks, and the cracks are more straightforward to expand. At the same time, due to the excessive accumulation of $CO_2$ in the reservoir near the near well, the rock and the fluids in the area are in a relatively saturated state. Under this state, even though it is easy to produce cracks in the rock, the effect of the fracture expansion is not significant, but it leads to the formation of long cracks. In this state, although the rock is easy to produce cracks, the effect on the next step of crack propagation is not notable, which leads to the excessive accumulation of $CO_2$ in this region. In summary, it is crucial to consider the volume of gas injection when pursuing both the effectiveness of fracturing and the economy of fracturing.




(**a**) injection of 0 days (**b**) injection of 30 days

(**c**) injection of 90 days (**d**) injection of 180 days

(**e**) injection of 360 days scale

**Figure 5.** Plan view of the extent of $CO_2$ waves in the reservoir.

## 6. Field Application and Optimization Results

The formation closure pressure is one of the key factors affecting the fracturing effect. When the closure pressure exceeds 40 MPa, the crushing rate of large-size proppant increases significantly, which will lead to the increase in pore throat plugging rate and then affect the conductivity of oil and gas. At the same time, the conductivity of the combined particle size is much larger than that of the single particle size [21]. The closure pressure of the formation in this block is as high as 47 MPa. Therefore, the selection of combined particle size can effectively improve the stability of the proppant, reduce the crushing rate and ensure the smooth diversion of oil and gas. The specific construction plan is to pump the ceramsite 40/70 mesh first and then pump the ceramsite 30/50 mesh. Well P1 is a production well located in Block X, which is exploited by vertical well fracturing. The fracturing section is 3474.1–3484.8 m, the total injected fracturing fluid and carbon dioxide are 854 $m^3$ and 600 $m^3$, respectively, and the combined particle size ceramsite is 28 $m^3$. The highest sand ratio reaches 10%, and the average sand ratio is 6%. These parameters have reached the leading level in China. The fracturing construction data are shown in Table 5, and the fracturing construction curve of well P1 is shown in Figure 6. The sand ratio represents the ratio of the volume of proppant to the volume of fracturing fluid. Through this fracturing, the production of well P1 has changed significantly. Compared with before and after fracturing, the daily liquid production is 1.6 t, the daily gas production has increased

by 820 $m^3$, and the daily oil production has increased by 0.7 t. The effect of single-well production is remarkable, which has made an important contribution to the oil and gas production in this block. This not only proves the scientificity and effectiveness of our fracturing scheme but also provides valuable experience and reference for the subsequent development of similar blocks.

**Table 5.** Fracturing construction data.

| Stage Name | Types of Liquid | Stage Fluid ($m^3$) | Pumping Displacement ($m^3$/min) | Pumping Pressure (Mpa) |
|---|---|---|---|---|
| Pressure test | Active water | 4.8 | 1.8 | 44 |
| Ahead fluid | $CO_2$ | 297 | 3 | 82.3 |
| Sand-carrying fluid | $CO_2$ | 539 | 3 | 82.9–71.9 |
| Replacement fluid | $CO_2$ | 18 | 3 | 33.5 |

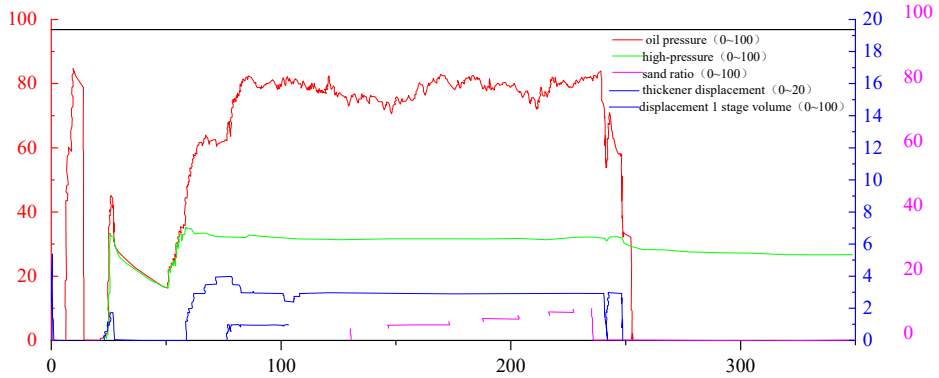



**Figure 6.** Fracturing construction curve for well P1.

## 7. Conclusions

(1) $CO_2$ quasi-dry fracturing technology ingeniously combines the advantages of $CO_2$ dry fracturing and water-based fracturing. It can achieve large-scale sanding without relying on closed sand mixing tank equipment and is suitable for the efficient development of complex reservoirs such as low porosity, low permeability, strong water sensitivity, and water lock.

(2) In the selection of the fracturing fluid formulation system, the fracturing fluid formulation system is 70% liquid $CO_2$ + 30% water, and 1.2% APQD-6 and 1.2% APFR-2 are added. The system has excellent viscoelastic properties, temperature shear resistance and sand suspension performance. The formulation meets the strict requirements of drag reduction and sand-carrying integration in $CO_2$ quasi-dry fracturing of low-porosity and low-permeability reservoirs.

(3) The results of carbon dioxide fracturing construction parameters are as follows: the construction displacement is 3 m3/min, and the fracture half-length is 206.2 m, which provides accurate guidance for the actual fracturing operation and helps to ensure the scientificity and effectiveness of the construction process.

(4) The analysis results of temperature and pressure in the reservoir and grid show that the temperature's response to CO2 injection is rapid, and its influence is significantly greater than that of pressure. In addition, in the early stage of accumulation, the temperature and pressure of the near-well reservoir show extremely high sensitivity to $CO_2$ injection. This finding provides a deep understanding of the migration and distribution of $CO_2$ in reservoirs.

**Author Contributions:** Writing—original draft preparation, writing—review, and editing, W.Y.; supervision, M.F.; methodology, Y.W.; investigation, J.L.; data curation, G.L. All authors have read and agreed to the published version of the manuscript.

**Funding:** Supported by the National Natural Science Foundation of China (NSFC) under Grant No. 52104018.

**Data Availability Statement:** Data are contained within the article.

**Conflicts of Interest:** The authors declare no conflicts of interest.

## References

1. Xiao, B.; Jiang, T.; Zhang, S. Numerical Simluation on Proppant Transport of Liquid Carbon Dioxide in Vertical Fracture. *Sci. Technol. Eng.* **2018**, *18*, 186–190.
2. Gou, B.; Ma, Y.; Liu, Z.; Zhou, C.; Wang, K. Research progress and prospect of numerical modeling for acid fracturing of heterogeneous car-bonate reservoirs. *Nat. Gas Ind.* **2019**, *39*, 87–98.
3. Luo, P.; Qiao, H.; Li, Z.; Huang, H.; Sun, X.; He, P. Leak off characteristics of supercritical $CO_2$ in lacustrine shale based on discrete fracture network model. *Sci. Technol. Eng.* **2020**, *20*, 146–152.
4. Gupta, D.V.S.; Bobier, D.M. The history and success of liquid $CO_2$ and $CO_2$/N2 fracturing system. In Proceedings of the SPE Unconventional Resources Conference/Gas Technology Symposium, San Diego, CA, USA, 8–11 November 1998; p. 40016.
5. Huang, C.; Huo, L.; Wu, C. Progress and prospect of CO, resource utilization technology based on unconventional oil and gas development. *Unconv. Oil Gas* **2022**, *9*, 1–9.
6. Barree, R.D.; Conway, M.W. *Experimental and Numerical Modeling of Convective Proppant Transport*; All Days; SPE-28564-MS; SPE: New Orleans, LA, USA, 1994.
7. Zhang, T.; Guo, J.C.; Liu, W. CFD Simulation of Proppant Transportation and Settling in Water Fracture Treatments. *J. Southwest Pet. Univ. (Nat. Sci. Ed.)* **2014**, *36*, 74–82.
8. Song, W.; Zhaozhong, Y.; Hua, L. Numerical Simulation Research of Proppant Transportation in Hydraulic Fracturing. *J. Pet. Gas* **2009**, *31*, 380–383+441.
9. Sun, H.; Su, W.; Wang, J.; Zhou, C.; Chen, P.; Xu, Y.; Zhou, R.; Zhang, C.; Du, Y. Progress and Prospect of Carbon Dioxide Fracturing Technology for Unconventional Oil and Gas Reservoirs. *Drill. Prod. Process* **2024**, *47*, 102–109.
10. Jia, Z. Research and field test of $CO_2$ quasi-dry fracturing technology. *Oil Prod. Eng.* **2024**, *3*, 29–34+91–92.
11. Zheng, Y.; Bai, X.; Luo, Y.; Yang, C.; Wang, Y. Research progress of unconventional oil and gas carbon dioxide fracturing technology. *China Pet. Chem. Ind. Stand. Qual.* **2019**, *39*, 221–224+226.
12. Li, S.; Zhang, S.; Zou, Y.; Zhang, X.; Ma, X.; Wu, S.; Zhang, Z.; Sun, Z.; Liu, C. Experimental study on the feasibility of supercritical $CO_2$-gel fracturing for stimulating shale oil reservoirs. *Eng. Fract. Mech.* **2020**, *238*, 107276. [CrossRef]
13. Zheng, B.; Qi, S.; Lu, W.; Guo, S.; Wang, Z.; Yu, X.; Zhang, Y. Experimental Research on Supercritical Carbon Dioxide Fracturing of Sedimentary Rock: A Critical Review. *Acta Geol. Sin.-Engl. Ed.* **2023**, *97*, 925–945. [CrossRef]
14. Song, W.; Ni, H.; Tang, P.; Zhang, S.; Gao, J.; Zhang, J.; Shen, B. Simulation of Supercritical Carbon Dioxide Fracturing in Shale Gas Reservoir. *J. Therm. Sci.* **2021**, *30*, 1444–1451. [CrossRef]
15. Luo, C. Research and application of $CO_2$ quasi-dry fracturing technology. *Pet. Nat. Gas Chem. Ind.* **2021**, *50*, 83–87.
16. Liu, G.; Bai, X.; Ma, Z.; Zhang, Y.; Yang, H. Research and application of quasi-dry fracturing technology for normal pressure mixed sand. *Drill. Fluid Complet. Fluid* **2021**, *38*, 375–379.
17. Wang, A.; Liu, X.; Sun, X.; Tang, Z.; Chu, W.; Cai, S. Fracturing technology for thin and poor layers in deep low permeability reservoirs in Zhongyuan Oilfield. *Drill. Prod. Technol.* **2012**, *35*, 70–71+11.
18. Wu, G.; Xu, Y.; Yang, Z.; Yang, L.; Zhang, J. Numerical simulation considering the effect of proppant and its embedding degree on the conductivity of propped fractures. *Nat. Gas Ind.* **2013**, *33*, 65–68.
19. Zang, Y.; Wang, H.; Wang, B.; Sun, J.; Wang, T.; Tian, G.; Shi, M.; Wu, Y.; Tian, S. Distribution characteristics of pre-$CO_2$ fracturing fluid in shale oil reservoirs in Ordos Basin. *J. Xi'an Pet. Univ. (Nat. Sci. Ed.)* **2024**, *39*, 55–61.
20. Zhao, X. Optimization of $CO_2$ Fracturing Parameters in Low Permeability Gas Reservoirs. Ph.D. Thesis, Southwest Petroleum University, Chengdu, China, 2018.
21. Han, W.; Zheng, Y.; Zhang, J.; Yang, Q.; Sun, Z.; Wei, Q. Evaluation and optimization of proppant in a block of Yanchang gas field. *Chem. Eng. Equip.* **2021**, *12*, 71–73. [CrossRef]

**Disclaimer/Publisher's Note:** The statements, opinions and data contained in all publications are solely those of the individual author(s) and contributor(s) and not of MDPI and/or the editor(s). MDPI and/or the editor(s) disclaim responsibility for any injury to people or property resulting from any ideas, methods, instructions or products referred to in the content.